Integrated Systems and Technologies

Cancer Research

Cell–Cell Adhesion and Cytoskeleton Tension Oppose Each Other in Regulating Tumor Cell Aggregation

Laure Saias[1,2], Aurélie Gomes[1,2], Martine Cazales[1,2], Bernard Ducommun[1,2,3], and Valérie Lobjois[1,2]

Abstract

Cell aggregation is frequently impaired during the growth of primary tumors and the formation of metastatic lesions. Cell aggregation depends on cell–cell adhesion; however, no rigorous approach exists to monitor and quantify it accurately in the absence of the confounding factors of cell–substrate adhesion and the resulting cell motility on the substrate. We report here a highly reproducible, automated, microscopy-based quantification of tumor-cell spheroid formation in the absence of cell–substrate adhesion and use it to characterize cell aggregation dynamics in the early steps of this process. This method is based on fluorescence and bright-field microscopy and on a custom MATLAB program to quantify automatically the cells' aggregation kinetics. We demonstrate that the cell–cell adhesion protein E-cadherin and the desmosome proteins DSG2 and DSC2 are important for aggregation. Furthermore, we show that inhibition or silencing of myosin IIa enhances aggregation, suggesting that cytoskeleton tension inhibits tumor cell aggregation. This work opens new avenues to study the principles that govern multicellular aggregation, to characterize the aggregation properties of various tumor cell types, as well as to screen for drugs that inhibit or promote aggregation. *Cancer Res; 75(12); 2426–33. ©2015 AACR.*

Introduction

Tumor cell invasion and metastasis are the major obstacles to successful treatment of cancer patients. Metastatic dissemination is associated with deregulation of numerous cell processes, including the ability of tumor cells to aggregate (1). Both pro- and anti-aggregation forces contribute to promoting cancer dissemination: loss of cohesion forces in the primary tumor allows individual cancer cells or small groups of cells to escape into the lymphatic and circulatory systems (2), whereas the increased cell–cell adhesiveness of metastatic cells allows them to form multicellular homotypic aggregates, which have an increased chance of survival once detached from the primary tumor (3). Formation of these malignant cell aggregates also enhances their probability of interacting with endothelial cells in small capillaries and of their extravasation into surrounding tissues, which are necessary steps for metastasis (4, 5).

Numerous cell–cell adhesion proteins, notably proteins of the cadherin superfamily, are involved in cell aggregation. Deregulation of cell aggregation in metastatic cells is reported to result from loss of functional E-cadherin accompanied by a gain of expression of N-cadherin (6), differential adhesion to the extracellular matrix (7), or a response to inflammatory cytokines (8). A few studies also suggest that cell aggregation correlates inversely with tension in the cytoskeleton (9). Cell–cell adhesion and cytoskeleton tension have been studied extensively at the molecular scale, but describing the molecular events within single cells cannot alone predict the behavior of a multicellular population. How the interplay between cell–cell adhesion and cytoskeleton tension affects the aggregation at a multicellular scale still remains unclear (10).

So far, no rigorous methods have been reported to monitor and quantify cell aggregation kinetics. The study reported here aimed to characterize quantitatively how tumor cells aggregate at the multicellular scale by using a new, high-throughput method to quantify the kinetics of aggregation of tumor cell populations. This method involves automatic imaging combined with a custom-made automated image analysis procedure. To avoid the confounding factors of cell adhesion to substrate and migration on a matrix, we characterized the early steps of multicellular tumor spheroid formation on a poorly adhesive substrate. Using this approach, we have shown that in HCT116 colon cancer cells not only are E-cadherins involved in aggregation, but also other processes, such as desmosomal adhesion, work in parallel. Finally, we have shown that decreased cytoskeleton tension correlated with faster aggregation, suggesting that myosin IIa applies a counter force that slows down aggregation. This new approach may prove useful to decipher the principles that govern the kinetics of multicellular aggregation with the aim of developing new approaches to diagnose, assess, and treat progressive malignancies.

Materials and Methods

Production of the HCT116 H2B–mCherry expressing cell line

A cDNA encoding a histone H2B protein fused to the fluorescent protein mCherry (kindly provided by R. Tsien) was

[1]Université de Toulouse, ITAV-USR3505, Toulouse, France. [2]CNRS, ITAV-USR3505, Toulouse, France. [3]CHU de Toulouse, Toulouse, France.

Note: Supplementary data for this article are available at Cancer Research Online (http://cancerres.aacrjournals.org/).

Corresponding Authors: Valérie Lobjois, Centre Pierre Potier, ITAV-USR3505, 1 Place Pierre Potier, 31106 Toulouse 1, France. Phone: 33-582-99-10-47; E-mail: valerie.lobjois@itav.fr; Bernard Ducommun, bernard.ducommun@itav.fr

doi: 10.1158/0008-5472.CAN-14-3534

AACR

transferred to the pTRIP lentiviral shuttle vector. The resulting plasmid was used to produce lentiviral particles in 293FT embryonic kidney cells (Life Technologies) after calcium chloride tri-transfection together with pGag/pol and pVSV-G plasmids (provided by Vectorology platform, INSERM U1037). Seven hours after transfection, the DMEM+Glutamax (Life Technologies) medium supplemented with 10% fetal calf serum (FCS; Invitrogen) was replaced with serum-free OPTIMEM+Glutamax medium (Life Technologies). Lentiviral particles were harvested 48 hours later. HCT116 colorectal cancer cells (ATCC) were then transduced with the lentiviral particles at a multiplicity of infection (MOI) of 6 in the presence of 4 μg/mL protamine sulfate in OPTIMEM+Glutamax. Medium was replaced 7 hours later with DMEM+Glutamax +10% FCS. We thus obtained a cell line (HCT116-H2B–mCherry) stably expressing the H2B–mCherry fusion protein.

Cell culture and spheroid generation

The HCT116-H2B–mCherry and MDA-MB-231 cell lines (ATCC) were cultured in DMEM medium supplemented with 10% FCS and 100 U/mL penicillin/streptomycin. MCF7 cells (ATCC) were cultured in RPMI medium supplemented with 5% FCS and 1 μmol/L insulin. Cells were cultured in a humidified atmosphere of 5% CO_2 at 37°C. For CellMask Orange (Life Technologies) staining, cells growing on a plastic culture well were incubated for 15 minutes at 37°C with CellMask agent at 1 μg/mL, then rinced in PBS, trypsinized, and prepared for spheroid formation and image acquisition. Spheroids were prepared as described previously (11, 12). Briefly, cells were distributed into poly-HEMA–coated, round-bottomed 96-well plates at a density of 500 cells per well. The plates were centrifuged at 191 × *g* for 6 minutes. For imaging, culture medium was replaced by OptiMem (Invitrogen) supplemented with 5% FCS and 1% penicillin/streptomycin for HCT116 cells and MDA-MD-231 cells, or by DMEM-F12 supplemented with 1 μmol/L insulin, 10 nmol/L β-estradiol, epidermal growth factor (20 ng/mL; Invitrogen), B-27 Supplement (1×, Invitrogen) for MCF7 cells.

Reagents

RGD peptide and trypsin were purchased from Life Technologies. Antibodies against E-cadherin (mouse monoclonal IgG1 HECD-1 clone) and against myosin IIa (ab55456) were purchased from AbCam, and the antibody against DSG2 (mouse monoclonal IgG1 AH12.2 clone) was from Santa Cruz Biotechnology. The IgG1 control monoclonal antibody (3.12.i.22) was produced in the laboratory (13). CAR peptides (DSG2: LTGYALDARG; DSC2: IIAFATTPDG) were synthesized by Euromedex. Blebbistatin was purchased from Sigma.

siRNA transfection

ON-TARGETplus Human MHY9 siRNA and siRNA buffer were purchased from Thermo Fisher Scientific. Cells were cultured in 12-well plates and transfected with MYH9 siRNA (1 nmol/L) by using the Interferin reagent (Ozyme) following the manufacturer's procedure. Experiments were conducted 3 days after transfection.

Time-lapse experiments

Time-lapse video microscopy images were acquired over at least 20 hours (1 acquisition/15 minutes), by using an inverted wide-field Zeiss Axio Observer Z1 microscope fitted with a 0.3 N.A 10× objective and a CoolSNAP CDD camera (Roper scientific). At each time point and position, 10-μm spaced z-stacks of bright-field and mCherry fluorescence were acquired by using MetaMorph software.

Image processing and analysis for aggregation process quantification

At each time point, and for each aggregate, maximal projections of the mCherry images were obtained by using the ImageJ software. The principal steps of the algorithm to detect and measure the aggregate over time with a custom-made MATLAB procedure were: (i) selection of the focus plane of transmission images where the aggregate is the clearest by maximizing relative standard deviation (SD) of the intensity, (ii) binarization of mCherry projections and of the selected transmission plane using the *edge* function, (iii) calculation of the final binarized image by multiplying pixel by pixel the two previous binarized images, (iv) detection by *bwboundaries* function and tracking of the object of interest at each time point by selection on size and position, (v) saving of the object's outline, and (vi) calculation of the characteristic parameters (coordinates of the center, area). The MATLAB code and a tutorial are available in Supplementary Data.

Immunofluorescent staining

Cells grown on coverslips for 3 days, were washed in PBS, and fixed for 5 minutes in methanol at −20°C, then washed, permeabilized in PSB containing 0.5% Triton X-100 for 5 minutes at room temperature, and incubated in PBS containing 5% FCS for 1 hour at room temperature. For immunofluorescent staining of spheroid frozen sections, spheroids grown for 7 days were washed in PBS, fixed for 3 hours in formalin at 4°C, incubated overnight in sucrose at 15%, and then for 3 hours in sucrose at 30% at 4°C. Spheroids were then embedded in OCT (Tissue-Tek) in cryomolds, flash-frozen, and 8-μm cryosections were prepared using a Leica CM1950 CryoStat. Sections were placed under vacuum overnight, stored at −20°C for 12 hours, rehydrated at room temperature in PBS for 20 minutes, postfixed in formalin for 15 minutes, washed in PBS for 10 minutes, and permeabilized in PBS containing 0.5% BSA and 0.5% Triton X-100 for 30 minutes. Frozen sections or cells fixed on coverslips were incubated overnight at 4°C with antibodies against E-cadherin (1/400, clone HECD-1; Abcam), DSG2 (1/800, clone AH12.2; Santa Cruz Biotechnology), or myosin IIa (1/1,000, clone ab55456; Abcam) in PBS containing 5% FCS. After washes in PBS containing 0.1% Triton X-100, goat anti-mouse Alexa Fluor 594 antibodies (Molecular Probes, 1/800) were applied for 1.5 hours at room temperature. DNA was stained with DAPI at 1 μg/mL, for 10 minutes at room temperature.

Results

Cells spontaneously form 3D aggregates on poorly adhesive substrates

To investigate the tumor cell aggregation process independently of cell migration or matrix adhesion, we chose to study the formation of multicellular tumor spheroids, which are widely used as an *in vitro* model for microtumors (14–17). We used a colon adenocarcinoma cell line, HCT116, engineered to express a histone H2B–mCherry fluorescent fusion protein,

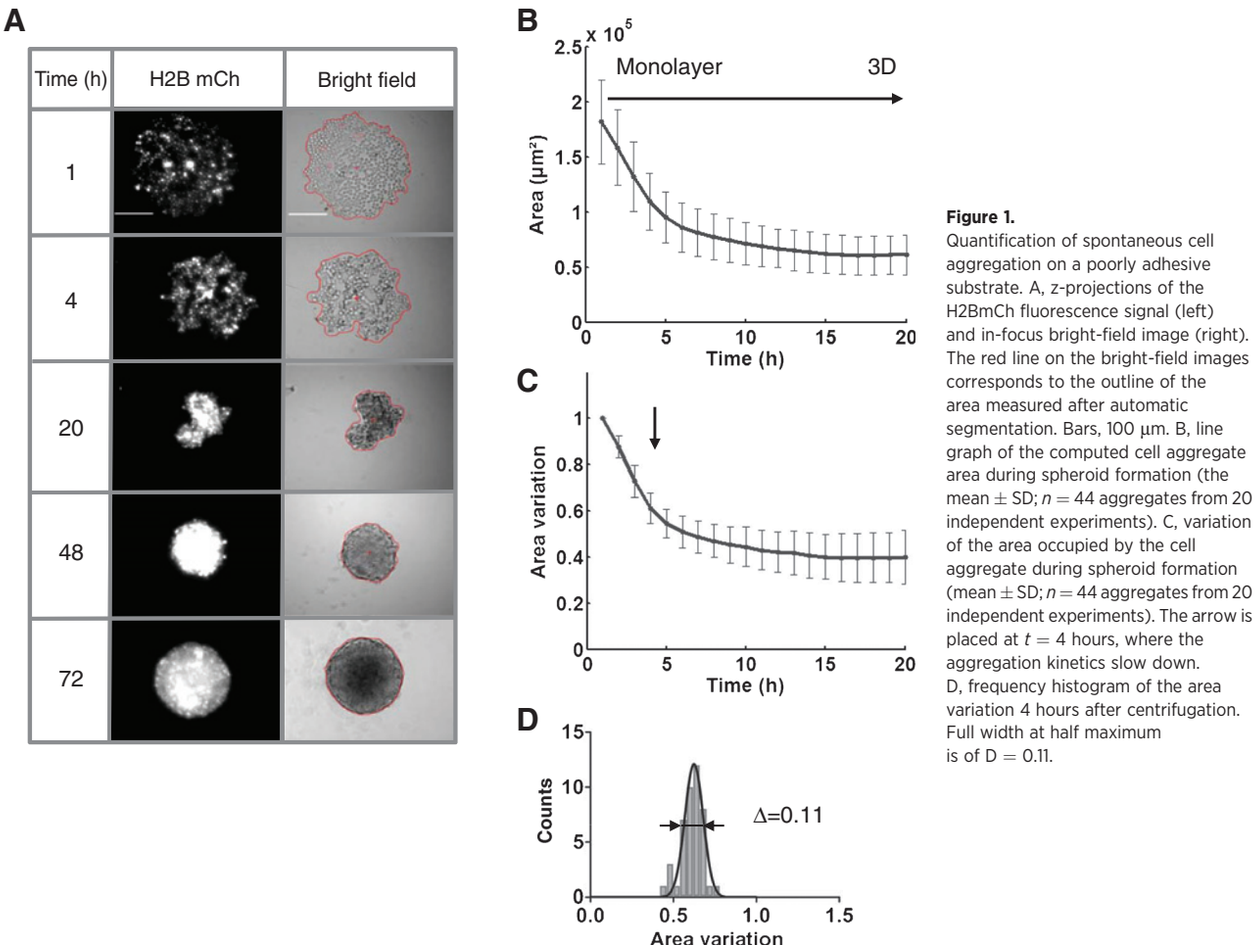

Figure 1.
Quantification of spontaneous cell aggregation on a poorly adhesive substrate. A, z-projections of the H2BmCh fluorescence signal (left) and in-focus bright-field image (right). The red line on the bright-field images corresponds to the outline of the area measured after automatic segmentation. Bars, 100 μm. B, line graph of the computed cell aggregate area during spheroid formation (the mean ± SD; $n = 44$ aggregates from 20 independent experiments). C, variation of the area occupied by the cell aggregate during spheroid formation (mean ± SD; $n = 44$ aggregates from 20 independent experiments). The arrow is placed at $t = 4$ hours, where the aggregation kinetics slow down. D, frequency histogram of the area variation 4 hours after centrifugation. Full width at half maximum is of D = 0.11.

which allowed us to visualize the cells by fluorescence microscopy (Fig. 1A). Cells were distributed into U-shaped 96-well plates treated to prevent cell adhesion to the surface (12, 18), so that the cells could not adhere nor migrate on the substrate by applying motile forces. The cells were concentrated by gentle centrifugation at the bottom of the wells where they could aggregate to form spheroids.

One hour after centrifugation, a monolayer of individual cells was visible (Fig. 1A). Over the next 20 hours, the cells spontaneously and progressively adhered to one another to form a cohesive aggregate with no space between them before starting to proliferate (Supplementary Movie S1). After 48 hours, the cells in the aggregates had begun to organize and to adopt a regular round shape (Fig. 1A). After 72 hours, a spheroid had formed with a distinct, regular boundary and a spherical 3D shape (data not shown). To study the period corresponding to the aggregation process itself, we focused the rest of our analyses on the first 20 hours after centrifugation.

Automated quantification of the kinetics of cell aggregation

To quantify the aggregation kinetics of the cells, we measured the area of the surface occupied by the cells by a dedicated MATLAB procedure that automatically detects and tracks the forming cell aggregate using bright-field and fluorescence time-lapse microscopy (Supplementary Fig. S1A). This approach allowed us to determine the outline of the area occupied by the cell population as accurately as possible. Briefly, bright-field and fluorescence images were binarized and combined (Supplementary Movie S1). Subsequent image segmentation enabled detection and tracking of the aggregate at each time point (Supplementary Movie S2). Other data, such as the aggregate center and area, were computed automatically (for further details; see Materials and Methods). This method enabled us to analyze the aggregation kinetics of about 25 samples in 2 hours, from raw image selection to aggregate area measurements.

Area measurements showed two phases of cell aggregation (Fig. 1B). During the first 5 hours, the area decreased rapidly as the cells entered into contact and started to form a dense monolayer. The second phase started when this rapid decrease in area began to slow down and stabilize. This phase correlated with the transition from a 2D to a 3D structure, that is, when the cells began to form a structure two or more cell layers thick.

To compare the aggregation kinetics in different wells, we normalized the measured area after the observation time to the area occupied by the cells 1 hour after centrifugation ("area variation," Fig. 1C). The mean value of the area variation 4 hours after the centrifugation step was 0.62 ± 0.065 SD ($n = 44$ from 20 independent experiments). The low SD as well as the low full width at half maximum value (0.11) of the area variation

distribution showed the reproducibility of our method (Fig. 1D). We used this area variation parameter to quantify the cell aggregation kinetics in all the following experiments performed on HCT116 cells. To use the same procedure to study MCF7 and MDMB231 cells that were not genetically modified to express a fluorescent reporter, we stained the cell membranes with the fluorescent marker CellMask Orange. The kinetics of aggregation were similar for cells treated or not with this marker (data not shown).

Together, these data demonstrate that our method is highly reproducible and is an useful tool to quantify collective cell aggregation kinetics.

Cell aggregation on a poorly adhesive substrate is independent of integrins

We aimed to study cell aggregation independently of cell migration or matrix adhesion. If the cell aggregation we observed above on a poly-HEMA–treated antiadhesive surface was truly independent of cell migration or matrix adhesion, it should be independent of integrins. We tested this hypothesis by blocking integrin-dependent cell–matrix adhesions with an Arg–Gly–Asp (RGD) peptide, which inhibits integrin–extracellular matrix interactions (19, 20). The efficacy of 0.5 mmol/L RGD peptide was first verified by showing its inhibitory effect on cell adhesion to traditional culture dishes (Supplementary Fig. S1B). In the aggregation assay, over the first 20 hours of aggregation 0.5 mmol/L RGD peptide had no significant effect on aggregate shape and area variation dynamics (Fig. 2 and Supplementary Fig. S1B). These data confirm that cells do not adhere to poly-HEMA–coated culture wells and that the aggregation process is independent of integrins.

E-Cadherins are not sufficient to complete collective cell aggregation

E-Cadherins are among the main molecules involved in cell–cell adhesion and inhibition of E-cadherins has been shown to inhibit cell aggregation (21). We used the aggregation assay described above to investigate the role of E-cadherins in cell aggregation during the early step of spheroid formation by blocking specifically homotypic E-cadherin–binding sites with a monoclonal anti–E-cadherin antibody (HECD-1 clone; refs. 21, 22). In the presence of this antibody, aggregation was slightly slower and less effective (Fig. 2): after 20 hours, the area variation was 54.4% higher in wells treated with the antibody against E-cadherin than it was in wells treated with the control irrelevant monoclonal antibody (3.12.i22), which does not interact with membrane proteins (Fig. 3A). We also studied the breast cancer cell lines MCF7 and MDA-MB-231 that are reported to express, respectively, high and very low levels of E-cadherin (confirmed in Supplementary Fig. S2; refs. 23, 24). MDA-MB-231 cells stained with CellMask Orange aggregated less than similarly stained MCF7 cells as determined by measurement of area variation: the area occupied by the MDA-MB-231 cells after 20 hours had decreased to only 65% of the area at 1 hour, whereas after 20 hours, MCF7 cells had aggregated to 20% of the area at 1 hour (Fig. 3B and C). When treated with the monoclonal antibody against E-cadherin, MDA-MB-231 cells showed no obvious difference in their aggregation when compared with untreated cells, consistent with these cells expressing very little E-cadherin, as previously reported (23, 24). In contrast, MCF7 cell aggregation was much more impaired by the antibody treatment. Together, these data show that E-cadherins probably participate in the early cell aggregation process during the formation of spheroids; however, as all three tumor cell lines treated with the anti–E-cadherin antibody retained their ability to aggregate to a certain extent (Fig. 3) and increasing the concentration of the antibody had no additional effect (data not shown), we conclude that E-cadherins are likely not the only factor driving this process.

Tumor cell aggregation depends on calcium-dependent protein–protein interactions

To investigate the other cellular mechanisms that might regulate cell aggregation, we first verified that proteins were necessary to control this process by adding 0.4% trypsin to the culture medium, which completely inhibited the aggregation process (Figs. 2 and 3A). As this inhibition was stronger than the effect of the anti–E-cadherin antibody, this suggests that other plasma membrane proteins or protein domains are involved in cell aggregation. Moreover, the complete absence of aggregation even at the earlier time points of the experiment suggests that the aggregation observed in this assay is not driven passively by gravitational forces, but that it relies on extracellular proteins and/or membrane proteins. As most of the protein interactions involved in cell–cell adhesion are calcium-

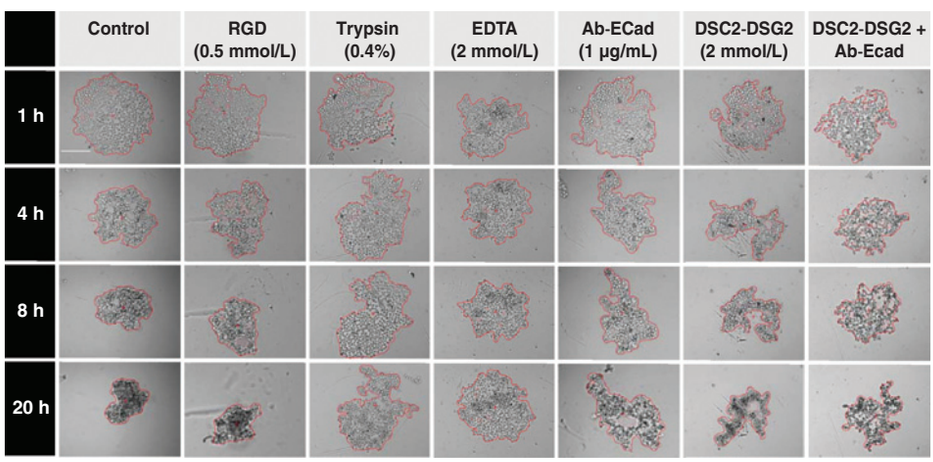

Figure 2.
Effects of various agents on cell aggregation. Representative in-focus bright-field images are shown for each experimental condition at the indicated time after centrifugation. The red line shows the segmented cell population used to calculate the area by our automated procedure.

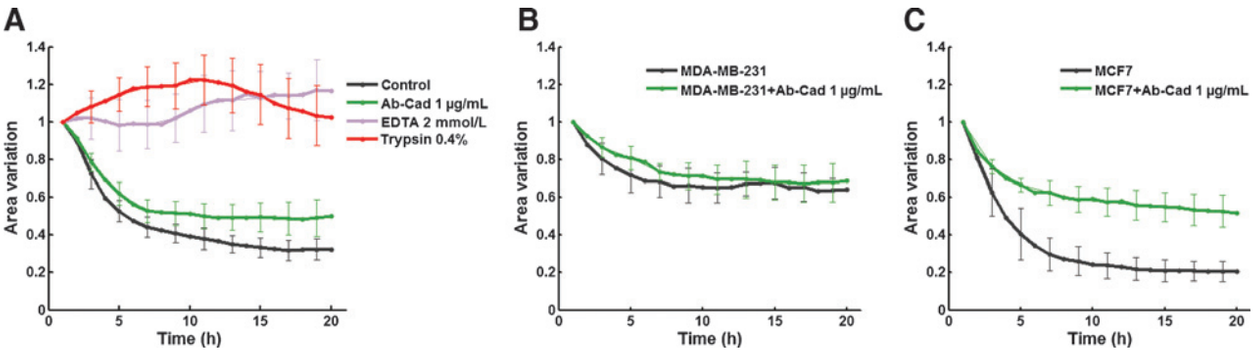

Figure 3.
E-Cadherin is not the only protein that drives aggregation. A, variation of the area occupied by HCT116 cells during the course of the aggregation assay when cells were treated with 3.12.i.22 antibody at 2 µg/mL (control; $n = 8$), with anti–E-cadherin antibody (Ab-Cad) at 1 µg/mL ($n = 29$), EDTA at 2 mmol/L ($n = 25$), or trypsin at 0.4% ($n = 36$). B, variation of the area occupied by MDA-MB-231 cells during aggregation when treated ($n = 33$), or not ($n = 31$), with anti–E-cadherin antibody at 1 µg/mL. C, variation of the area occupied by MCF7 cells during aggregation when treated ($n = 26$), or not ($n = 28$), with anti–E-cadherin antibody at 1 µg/mL. Values on the graphs correspond to mean ± SEM.

dependent, as are E-cadherin interactions (25–27), we examined the inhibitory effect of EDTA on cell aggregation. When the extracellular calcium concentration was decreased by adding 2 mmol/L EDTA to the culture medium, cell aggregation was also completely abolished (Fig. 2 and Fig. 3A). These data show that the aggregation observed in this assay likely involves additionnal calcium-dependent proteins other than E-cadherins.

Desmosomal proteins also coordinate cell aggregation

We next investigated whether other members of the cadherin superfamily may also be involved in cell aggregation. Desmogleins (DSG1–4) and desmocollins (DSC1–3) are cadherin superfamily proteins located in desmosomes. Previous studies have demonstrated that desmosomes are affected by calcium influx into the cell (28) and that homophilic and heterophilic interactions between DSC and DSG proteins generate cell aggregation (29, 30). It has also been shown that desmosomal protein expression may be altered during cancer development (31, 32) and may regulate cell proliferation (33). We found that DSG2 is expressed in HCT116 cells (Fig. 4A). To investigate the role of DSG2 and of its interaction partner DSC2 in the cell aggregation measured by our assay, we used peptides corresponding to the cell adhesion recognition (CAR) sites of DSG2 and DSC2 (29). Aggregation of HCT116 cells in the presence of these peptides was reduced (Fig. 4B) and the kinetics of cell aggregation were very similar to those in the presence of the antibody against E-cadherin. This suggests that E-cadherin–mediated and desmosome-mediated cell–cell adhesion both contribute to the aggregation process. When both the CAR peptides and the antibody against E-cadherin were added together to the culture medium there was an additive effect on cell aggregation, suggesting that adhesion through desmosomes and E-cadherin simultaneously coordinate collective cell aggregation.

Cytoskeleton tension acts as an inhibitor of cell aggregation

Adhesion proteins are coupled to the cytoskeleton in the cell cortex through complex assemblies of molecules (34, 35). Previous studies suggested that cell–cell adhesion and tension in the cell cortex may have opposing effects on cell aggregation (36, 37). Cell cortex tension is due mainly to the activity of myosin IIa (38). To investigate how cytoskeleton tension might influence cell aggregation in our assay, we studied the effect of inhibiting myosin IIa activity with a chemical inhibitor, blebbistatin, or by silencing the MYH9 gene using commercial, validated siRNAs (Supplementary Fig. S3A; ref. 39). Both approaches showed that the kinetics were faster and cell aggregation was more extensive when myosin IIa was inactivated (Fig. 5 and Supplementary

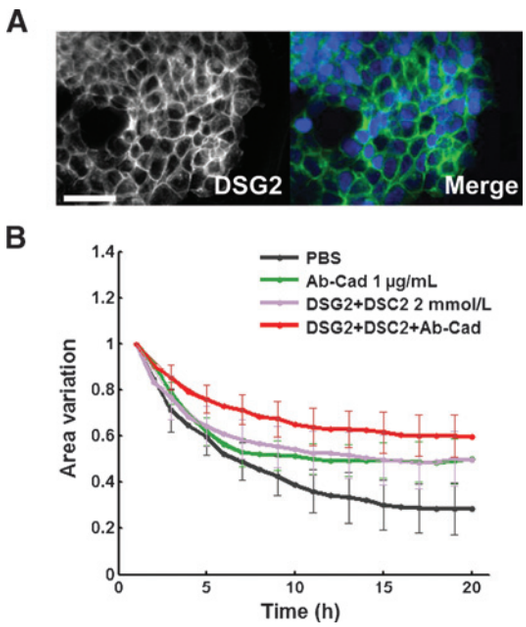

Figure 4.
E-Cadherin and desmosome proteins coordinate aggregation. A, left, immunofluorescence microscopy of HCT116 cells stained for DSG2; right, a merged image of the DSG2 signal (green) and DAPI staining of the nuclei (blue). Bar, 50 µm. B, variation of the area occupied by HCT116 cells during aggregation when cells were treated with 20% PBS (control; $n = 24$) or with 2 mmol/L peptides that block the function of DSG2 and DSC2 ($n = 29$), or with both 2 mmol/L peptides against DSG2 and DSC2 and anti–E-cadherin antibody at 1 µg/mL ($n = 20$). (As the DSC2 and DSG2 peptides were rehydrated in PBS, an equivalent volume of PBS was added to the control as was added to the peptide-treated cells.)

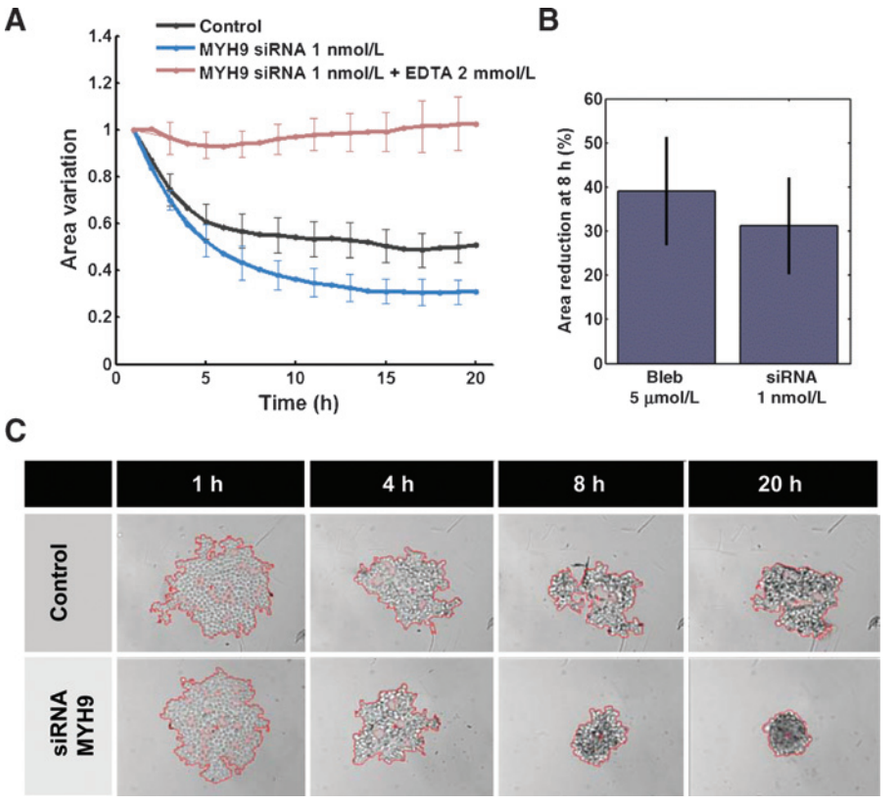

Figure 5.
Cytoskeleton tension acts as an inhibitor of cell aggregation. A, variation of the area occupied by HCT116 cells during the course of the aggregation assay for nontreated cells ($n = 17$) or cells that were transfected three days previously with MYH9 siRNA 1 nmol/L ($n = 28$), or for transfected cells treated with 2 mmol/L EDTA ($n = 22$). B, bar graph showing the reduction of the area occupied by the cells 8 hours after centrifugation, for cells either transfected with 1 nmol/L MYH9 siRNA three days previously or treated with 5 µmol/L blebbistatin compared with nontreated cells. C, representative segmented areas of in-focus bright-field images of nontreated HCT116 cells (control) and cells transfected with MYH9 siRNA.

Fig. S3B and S3C). When cell–cell adhesion was inhibited by adding EDTA or trypsin (data not shown) to MYH9 siRNA-treated cells, however, aggregation was totally inhibited (Fig. 5A). These data suggest that cytoskeleton tension due to myosin IIa acts as an inhibitor of cell aggregation, and that the integrity of membrane adhesion proteins remains a mandatory condition to drive the aggregation process.

Discussion

Quantification of the aggregative properties of cancer cells could help to predict their metastatic aggressiveness and also their response to drugs. Although the molecular bases of cell migration and cell–cell adhesion have been widely studied, they do not necessarily help us to predict the collective behavior of groups of cells. Here, we describe an easily implemented, automated method to characterize and quantify cell aggregation and we demonstrate the dependence of aggregation on cadherin superfamily proteins.

Cell aggregation forces, mainly produced by homotypic cell–cell adhesion, can be counterbalanced by other forces such as cell migration (due to matrix adhesion and motility forces). Thus, to characterize accurately the abilities of cancer cells to aggregate, one must uncouple these counterbalancing forces. Our method uses an experimental set-up that totally prevents cell adhesion to the substrate. In these conditions, the only force driving cell movement is cell–cell adhesion, resulting in cell aggregation.

Using this strategy, we present here a new quantitative method based on automatic image segmentation to quantify collective cell aggregation. We developed an automatic procedure based on MATLAB to detect, track cells and quantify their aggregation kinetics as they form spheroids. We show that this strategy can be used on genetically modified cells expressing a fluorescent reporter as well as on unmodified MCF-7 and MDA-MB231 stained with a fluorescent marker.

We used primarily the colorectal cancer cell line HCT116 as a model cell type to quantify cell aggregation. We treated the cells with multiple agents to show that aggregation was an active process, dependent on membrane proteins, and sensitive to calcium concentration. Treatment with a specific antibody against E-cadherin proved that this cell adhesion protein participates in the process but cannot alone complete it. We have shown that other proteins, such as desmosomal DSG2 and DSC2, also participate in the aggregation process simultaneously with and in addition to E-cadherin. Even when both E-cadherin- and DSC2/DSG2-mediated cell–cell adhesion was inhibited, however, cell aggregation was not entirely abolished. This suggests that other proteins may also be involved. Other cadherins, such as N- and P-cadherin and other desmosomal adhesion proteins (such as DSG1, DSG3, DSG4, DSC1 and DSC3), might take part in this process as their activities are associated with cancer development (1, 6, 22, 30, 40). Their involvement requires further investigation.

We also found that cytoskeleton tension, generated by myosin IIa activity, acts as an inhibitor of cell aggregation. This observation is consistent with other studies showing that E-cadherin–mediated adhesion is limited by the mechanical anchoring of E-cadherin to the cell cortex (36, 37). On the basis of our findings and previous studies, we propose a model in which the activity of myosin IIa disrupts cell–cell adhesion (36), thus inhibiting aggregation. These weak cell–cell contacts due to myosin IIa activity

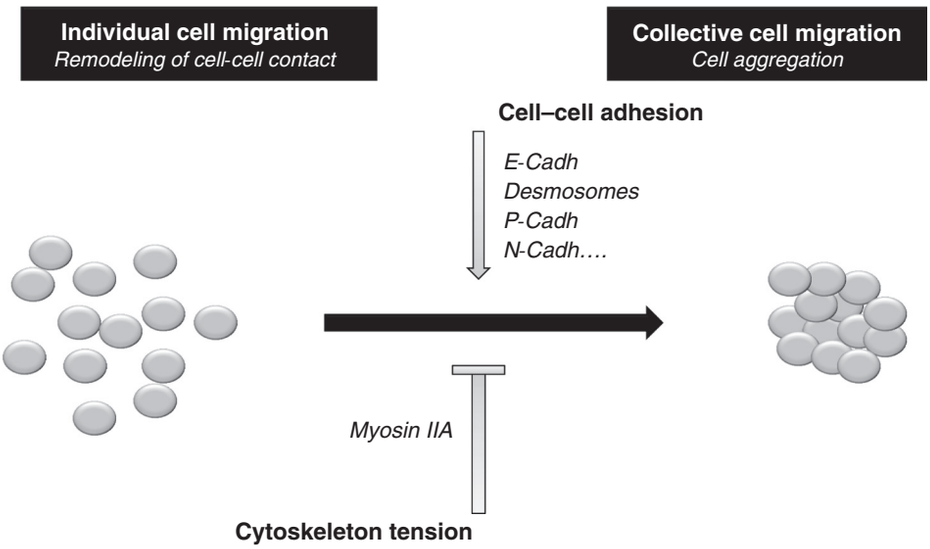

Figure 6.
Schematic of the proposed model showing the opposing roles played by cell–cell adhesion forces and cytoskeleton tension on cell aggregation.

might help cells to remodel their contacts more easily and favor their motiility. Increased myosin IIa activity might then enhance individual cell migration (Fig. 6). This interpretation is also consistent with studies suggesting that cytoskeleton tension controls cell–cell contact formation (37). In contrast, decreased myosin IIa activity would increase the strength of cell–cell contacts and favor the formation of group of cells. Interestingly, a previous study reported the opposite effect of myosin IIa on cell adhesion to the ECM; it concluded that integrin-dependent actomyosin traction force mediates the disruption of cell–cell adhesion during epithelial cell scattering (36). Decreased myosin IIa activity would inhibit maturation of adhesion to the ECM and increase migration velocity (41–43). Thus, decreased myosin IIa activity might favor both migration and cohesion of groups of tumor cells in ECM, which may contribute to tumor dissemination.

If cytoskeleton function influences cell–cell adhesion, this suggests that myosin IIa may be important in tumor development. A recent review discussed paradoxical findings showing that myosin IIa may have both a tumor-suppressor activity in squamous cell carcinomas and also an invasion-promoting activity in some cancer cell lines (38). Considering the opposing roles of myosin IIa on cell–ECM adhesion and cell–cell adhesion discussed above, we suggest that this paradox might arise from the fact that the tumor-suppressor activity was measured in situations where cells were migrating on a matrix (so myosin IIa activity would slow cell motion on the ECM), whereas the invasion-promoting activity was measured in a situation where cells were invading an epithelial tissue (so myosin IIa activity would inhibit mature cell–cell adhesion and favor cell motion in epithelial tissue). The roles of the actomyosin cytoskeleton in cell migration in epithelial tissues and on ECM have been studied broadly (44, 45), but more and more studies tend to show that myosin IIa activity might have antagonist effects on those processes (35). The environment directly in contact with the cells, whether ECM or other epithelial cells, is important for the regulation of cell migration. Further studies will be necessary to determine definitively the role of myosin IIa in tumor dissemination.

The experimental approach reported here can be used as a quantitative assay to test the aggregative properties of various cell types and it would be of great interest to investigate whether there is a correlation between their aggregative dynamics and their metastatic potential. Also, this assay could be useful to test the efficacy of drugs on collective cell aggregation and tumor formation.

Disclosure of Potential Conflicts of Interest

No potential conflicts of interest were disclosed.

Authors' Contributions

Conception and design: L. Saias, B. Ducommun, V. Lobjois
Development of methodology: L. Saias
Acquisition of data (provided animals, acquired and managed patients, provided facilities, etc.): L. Saias, A. Gomes, M. Cazales
Analysis and interpretation of data (e.g., statistical analysis, biostatistics, computational analysis): L. Saias, A. Gomes, B. Ducommun, V. Lobjois
Writing, review, and/or revision of the manuscript: L. Saias, B. Ducommun, V. Lobjois
Administrative, technical, or material support (i.e., reporting or organizing data, constructing databases): L. Saias
Study supervision: B. Ducommun, V. Lobjois

Acknowledgments

The authors thank Odile Mondésert for initiating this work, the assistance of the TRI-Genotoul and ITAV imaging facilities (Toulouse, France), and Dr. D. Garrod (University of Manchester, Manchester, United Kingdom) for helpful advice on the desmosomal CAR peptide experiments. The authors are grateful to the members of our group for discussions and for their support of this project; Dr. Carol Featherstone for editing the article.

Grant Support

L. Saias is a recipient of a postdoctoral fellowship from the Fondation ARC. This work was supported by the Fondation pour la Recherche Médicale (Equipe labellisée 2011) and the ANR (12-BSV5-0008-01).

The costs of publication of this article were defrayed in part by the payment of page charges. This article must therefore be hereby marked *advertisement* in accordance with 18 U.S.C. Section 1734 solely to indicate this fact.

Received December 4, 2014; revised February 25, 2015; accepted March 17, 2015; published OnlineFirst April 8, 2015.

References

1. Usui A, Ko SY, Barengo N, Naora H. P-cadherin promotes ovarian cancer dissemination through tumor cell aggregation and tumor-peritoneum interactions. Mol Cancer Res 2014;12:504–13.
2. Hanahan D, Weinberg RA. The hallmarks of cancer. Cell 2000;100:57–70.
3. Glinsky GV. Anti-adhesion cancer therapy. Cancer Metastasis Rev 1998; 17:177–85.
4. Glinsky VV, Glinsky GV, Glinskii OV, Huxley VH, Turk JR, Mossine VV, et al. Intravascular metastatic cancer cell homotypic aggregation at the sites of primary attachment to the endothelium. Cancer Res 2003;63:3805–11.
5. Hsu J-W, Yasmin-Karim S, King MR, Wojciechowski JC, Mickelsen D, Blair ML, et al. Suppression of prostate cancer cell rolling and adhesion to endothelium by 1?,25-dihydroxyvitamin D3. Am J Pathol 2011;178: 872–80.
6. Li G, Satyamoorthy K, Herlyn M. N-cadherin-mediated intercellular interactions promote survival and migration of melanoma cells. Cancer Res 2001;61:3819–25.
7. Young T-H, Tu H-R, Chan C-C, Huang Y-C, Yen M-H, Cheng N-C, et al. The enhancement of dermal papilla cell aggregation by extracellular matrix proteins through effects on cell-substratum adhesivity and cell motility. Biomaterials 2009;30:5031–40.
8. Geng Y, Chandrasekaran S, Hsu J-W, Gidwani M, Hughes AD, King MR. Phenotypic switch in blood: effects of pro-inflammatory cytokines on breast cancer cell aggregation and adhesion. PLoS ONE 2013;8:e54959.
9. Derycke L, Stove C, Vercoutter-Edouart A-S, De Wever O, DollÈ L, Colpaert N, et al. The role of non-muscle myosin IIA in aggregation and invasion of human MCF-7 breast cancer cells. Int J Dev Biol 2011;55:835–40.
10. Pope MD, Asthagiri AR. Short-lived, transitory cell–cell interactions foster migration-dependent aggregation. PLoS ONE 2012;7:e43237.
11. Ivascu A, Kubbies M. Rapid generation of single-tumor spheroids for high-throughput cell function and toxicity analysis. J Biomol Screen 2006; 11:922–32.
12. Laurent J, Frongia C, Cazales M, Mondésert O, Ducommun B, Lobjois V. Multicellular tumor spheroid models to explore cell cycle checkpoints in 3D. BMC Cancer 2013;13:73.
13. Cazales M, Quaranta M, Lobjois V, Jullien D, Al Saati T, Delsol G, et al. A new mitotic-cell specific monoclonal antibody. Cell Cycle 2008;7: 267–8.
14. Fennema E, Rivron N, Rouwkema J, van Blitterswijk C, de Boer J. Spheroid culture as a tool for creating 3D complex tissues. Trends Biotechnol 2013;31:108–15.
15. Hirschhaeuser F, Menne H, Dittfeld C, West J, Mueller-Klieser W, Kunz-Schughart LA. Multicellular tumor spheroids: an underestimated tool is catching up again. J Biotechnol 2010;148:3–15.
16. Kunz-Schughart LA, Freyer JP, Hofstaedter F, Ebner R. The use of 3-D cultures for high-throughput screening: the multicellular spheroid model. J Biomol Screen 2004;9:273–85.
17. Sutherland RM. Cell and environment interactions in tumor microregions: the multicell spheroid model. Science 1988;240:177–84.
18. Tong JZ, De Lagausie P, Furlan V, Cresteil T, Bernard O, Alvarez F. Long-term culture of adult rat hepatocyte spheroids. Exp Cell Res 1992;200: 326–32.
19. Plow EF, Haas TA, Zhang L, Loftus J, Smith JW. Ligand binding to integrins. J Biol Chem 2000;275:21785–88.
20. Ruoslahti E. RGD and other recognition sequences for integrins. Ann Rev Cell Dev Biol 1996;12:697–715.
21. Bracke ME, Vyncke BM, Bruyneel EA, Vermeulen SJ, De Bruyne GK, Van Larebeke NA, et al. Insulin-like growth factor I activates the invasion suppressor function of E-cadherin in MCF-7 human mammary carcinoma cells *in vitro*. Br J Cancer 1993;68:282–9.
22. Shimoyama Y, Hirohashi S, Hirano S, Noguchi M, Shimosato Y, Takeichi M, et al. Cadherin cell-adhesion molecules in human epithelial tissues and carcinomas. Cancer Res 1989;49:2128–33.
23. Frixen UH, Behrens J, Sachs M, Eberle G, Voss B, Warda A, et al. E-cadherin-mediated cell-cell adhesion prevents invasiveness of human carcinoma cells. J Cell Biol 1991;113:173–85.
24. Sommers CL, Byers SW, Thompson EW, Torri JA, Gelmann EP. Differentiation state and invasiveness of human breast cancer cell lines. Breast Cancer Res Treat 1994;31:325–35.
25. Grunwald GB. The structural and functional analysis of cadherin calcium-dependent cell adhesion molecules. Curr Opin Cell Biol 1993;5:797–805.
26. Kemler R, Ozawa M, Ringwald M. Calcium-dependent cell adhesion molecules. Curr Opin Cell Biol 1989;1:892–7.
27. Koch AW, Pokutta S, Lustig A, Engel J. Calcium binding and homoassociation of E-cadherin domains. Biochemistry 1997;36:7697–705.
28. Hobbs RP, Amargo EV, Somasundaram A, Simpson CL, Prakriya M, Denning MF, et al. The calcium ATPase SERCA2 regulates desmoplakin dynamics and intercellular adhesive strength through modulation of PKCα signaling. FASEB J 2011;25:990–1001.
29. Runswick SK, O'Hare MJ, Jones L, Streuli CH, Garrod DR. Desmosomal adhesion regulates epithelial morphogenesis and cell positioning. Nat Cell Biol 2001;3:823–30.
30. Tselepis C, Chidgey M, North A, Garrod D. Desmosomal adhesion inhibits invasive behavior. Proc Natl Acad Sci U S A 1998;95:8064–9.
31. Chidgey M, Dawson C. Desmosomes: a role in cancer? Br J Cancer 2007;96:1783–7.
32. Kundu ST, Gosavi P, Khapare N, Patel R, Hosing AS, Maru GB, et al. Plakophilin3 downregulation leads to a decrease in cell adhesion and promotes metastasis. Int J Cancer 2008;123:2303–14.
33. Kamekura R, Kolegraff KN, Nava P, Hilgarth RS, Feng M, Parkos CA, et al. Loss of the desmosomal cadherin desmoglein-2 suppresses colon cancer cell proliferation through EGFR signaling. Oncogene 2013;33:4531–6.
34. Bershadsky A. Magic touch: how does cell-cell adhesion trigger actin assembly? Trends Cell Biol 2004;14:589–93.
35. Conti MA, Adelstein RS. Nonmuscle myosin II moves in new directions. J Cell Sci 2008;121:11–8.
36. de Rooij J, Kerstens A, Danuser G, Schwartz MA, Waterman-Storer CM. Integrin-dependent actomyosin contraction regulates epithelial cell scattering. J Cell Biol 2005;171:153–64.
37. Maître J-L, Berthoumieux H, Krens SFG, Salbreux G, Jlicher F, Paluch E, et al. Adhesion functions in cell sorting by mechanically coupling the cortices of adhering cells. Science 2012;338:253–6.
38. Ouderkirk JL, Krendel M. Non-muscle myosins in tumor progression, cancer cell invasion, and metastasis. Cytoskeleton 2014;71:447–63.
39. Li Y, Friedmann DR, Mhatre AN, Lalwani AK. MYH9-siRNA and MYH9 mutant alleles: expression in cultured cell lines and their effects upon cell structure and function. Cell Motil Cytoskeleton 2008;65:393–405.
40. Brown L, Waseem A, Cruz IN, Szary J, Gunic E, Mannan T, et al. Desmoglein 3 promotes cancer cell migration and invasion by regulating activator protein 1 and protein kinase C-dependent-Ezrin activation. Oncogene 2013;33:2363–74.
41. Even-Ram S, Doyle AD, Conti MA, Matsumoto K, Adelstein RS, Yamada KM. Myosin IIA regulates cell motility and actomyosin-microtubule crosstalk. Nat Cell Biol 2007;9:299–309.
42. Sandquist JC, Swenson KI, Demali KA, Burridge K, Means AR. Rho kinase differentially regulates phosphorylation of nonmuscle myosin II isoforms A and B during cell rounding and migration. J Biol Chem 2006;281:35873–83.
43. Vicente-Manzanares M, Zareno J, Whitmore L, Choi CK, Horwitz AF. Regulation of protrusion, adhesion dynamics, and polarity by myosins IIA and IIB in migrating cells. J Cell Biol 2007;176:573–80.
44. DuFort CC, Paszek MJ, Weaver VM. Balancing forces: architectural control of mechanotransduction. Nat Rev Mol Cell Biol 2011;12:308–19.
45. Hoffman BD, Grashoff C, Schwartz MA. Dynamic molecular processes mediate cellular mechanotransduction. Nature 2011;475:316–23.